Bifurcation Instability Modulated by a Connecting Channel Leads to Periodic Water Partitioning in a Simple Channel Network

Gao, Weilun; Wang, Zheng Bing; Kleinhans, Maarten G.; Shao, Dongdong; Zhu, Zhenchang; Yang, Zhifeng

DOI
10.1029/2024WR037668

Publication date
2024

Document Version
Final published version

Published in
Water Resources Research

Citation (APA)
Gao, W., Wang, Z. B., Kleinhans, M. G., Shao, D., Zhu, Z., & Yang, Z. (2024). Bifurcation Instability Modulated by a Connecting Channel Leads to Periodic Water Partitioning in a Simple Channel Network. *Water Resources Research*, *60*(11), Article e2024WR037668. https://doi.org/10.1029/2024WR037668

Water Resources Research

RESEARCH ARTICLE
10.1029/2024WR037668

Bifurcation Instability Modulated by a Connecting Channel Leads to Periodic Water Partitioning in a Simple Channel Network

Weilun Gao[1], Zheng Bing Wang[2,3], Maarten G. Kleinhans[4], Dongdong Shao[5], Zhenchang Zhu[1,6], and Zhifeng Yang[1,6]

[1]Guangdong Basic Research Center of Excellence for Ecological Security and Green Development, Guangdong Provincial Key Laboratory of Water Quality Improvement and Ecological Restoration for Watersheds, School of Ecology, Environment and Resources, Guangdong University of Technology, Guangzhou, China, [2]Faculty of Civil Engineering and Geosciences, Delft University of Technology, Delft, The Netherlands, [3]Deltares, Delft, The Netherlands, [4]Department of Physical Geography, Utrecht University, Utrecht, The Netherlands, [5]State Key Laboratory of Water Environment Simulation and School of Environment, Beijing Normal University, Beijing, China, [6]Southern Marine Science and Engineering Guangdong Laboratory (Guangzhou), Guangzhou, China

Abstract Water and mass transport in distributary channel networks play an important role in nourishing fluvial and coastal wetlands, and are largely determined by the morphological configurations of channel bifurcations. While the morphological equilibrium of a single channel bifurcation has been extensively studied, the equilibrium configurations of channel networks with connecting channels linking the bifurcating branches, that is, the "bifurcation-connecting channel" units that are commonly found in rivers, deltas and estuaries, remain elusive. In this simple yet representative channel network of the "bifurcation-connecting channel" unit, we observed through numerical simulations an oscillatory water partitioning under moderate Shields stress and channel aspect ratio, in addition to the steady-state solutions reported in previous studies. The oscillatory water partitioning indicates a newly discovered periodic solution, which is an emergent behavior under constant boundary conditions. We found that the periodic solution is primarily due to the dynamic interactions between bifurcation instability and water surface slope advantage in the two branches modulated by the reversable discharges through the connecting channel, under moderate Shields stress and channel aspect ratio. In such cases, the developed slope advantage in the subordinate branch can suppress the deepening of the dominant branch and eventually lead to the shifting of the dominant branch. In contrast, the channel network attains a steady-state solution when the slope advantage or the bifurcation instability is dominant with relatively low and high Shields stress (or channel aspect ratio). Our results improve the understanding on the evolution and restoration of channel networks under increasing human interventions in global deltas.

Plain Language Summary In rivers, deltas and estuaries, multiple channels deliver water, sediment and nutrients to the fluvial and coastal wetlands and habitats. Where channels split at so-called bifurcations, water and sediment are divided depending on the shape of the channel and downstream flow conditions. The equilibrium configurations of a single bifurcation have been extensively explored. Specifically, the bifurcation could lead to symmetrical channels but more often asymmetry occurs, so that one downstream channel expands whilst the other tends to be abandoned. Here we add a connecting channel that cross-cuts the fork, and explore the equilibrium configurations in such a simple but representative network comprising a bifurcation plus a connecting channel. We found that this network exhibits oscillatory behavior in the division of flow and sediment over the branches and the depth of the branches, but on average remains symmetrical. However, when removing the connecting channel, the bifurcation would shift to an asymmetric configuration. Our results imply that the connecting channel can lead to a dynamic yet overall more uniform mass partitioning in distributary channel networks, which in turn affects critical functions such as wetland ecosystem nourishment. These findings also open up new ways to investigate channel networks where tides are important.

Key Points:

- Distinctive periodic and steady-state solutions exist in the channel network of the "bifurcation-connecting channel" unit
- The periodic solution is an emergent behavior with oscillatory water partitioning in the network under constant boundary conditions
- The periodic solution results from the bifurcation instability modulated by the reversing connecting channel

Supporting Information:

Supporting Information may be found in the online version of this article.

Correspondence to:

D. Shao and Z. Yang,
ddshao@bnu.edu.cn;
zfyang@gdut.edu.cn

Citation:

Gao, W., Wang, Z. B., Kleinhans, M. G., Shao, D., Zhu, Z., & Yang, Z. (2024). Bifurcation instability modulated by a connecting channel leads to periodic water partitioning in a simple channel network. *Water Resources Research*, *60*, e2024WR037668. https://doi.org/10.1029/2024WR037668

Received 14 APR 2024
Accepted 14 OCT 2024

1. Introduction

Distributary channel networks distribute water, sediments, nutrients, etc. to fluvial floodplains and coastal seas, and are critical for society and wetland ecosystems (Dong et al., 2020; Hiatt et al., 2018; Salter & Lamb, 2022; Shaw et al., 2021). In particular, predicting the morphological evolution of deltaic channel networks and

unraveling the mechanism leading to their equilibrium configurations are critical for the sustainability and resilience of river deltas, with important implications for implementing restoration projects such as river diversion to mitigate land loss in coastal wetlands (Hoitink et al., 2020; Moodie & Passalacqua, 2021; Tejedor et al., 2017). Therefore, the morphological evolution of channel networks has received extensive attention in recent decades (Edmonds & Slingerland, 2007; Gao et al., 2018; Jerolmack & Swenson, 2007; Ke et al., 2019; Konkol et al., 2022).

As a critical morphological unit in deltaic channel networks, channel bifurcation possesses different equilibrium configurations, that is, the two downstream branches can remain open in a symmetric or asymmetric configuration or one of them closes off (see the review by Edmonds et al. (2021) and Kleinhans et al. (2013)). Furthermore, these equilibrium configurations can be either stable or unstable (Bolla Pittaluga et al., 2003; Federici & Paola, 2003; Wang et al., 1995). A stable equilibrium configuration indicates that the bifurcation can recover the initial morphological configuration under small perturbations. In reality, the channel bifurcation would finally evolve to one of the stable equilibrium configurations largely depending on the initial conditions. Furthermore, water partitioning at a river bifurcation can change over time due to migrating bars or meander bends in the upstream channel (Bertoldi et al., 2009; Kleinhans & van den Berg, 2011) as well as in-channel net-deposition caused by river mouth progradation or relative sea level rise at the downstream boundary (Salter et al., 2018). However, bifurcation equilibrium has been mainly studied for a single channel bifurcation at reach scale thus far (Bolla Pittaluga et al., 2003, 2015; van Denderen et al., 2018; Wang et al., 1995).

Predicting the long-term morphological evolution and equilibrium configurations of large-scale complex channel networks consisting of multiple bifurcations/confluences remains challenging. One of the challenges is that the equilibrium configurations of multiple channel bifurcations can affect each other. Specifically, the equilibrium configuration of an upstream channel bifurcation determines the water discharge and sediment supply to the downstream bifurcation, which can thus affect the development of the equilibrium configuration of the downstream bifurcation. Further, a downstream confluence could also affect the equilibrium configurations of an upstream bifurcation by increasing/decreasing the water surface slope of the subordinate/dominant branch. Therefore, the interactions between bifurcations and confluences in a channel network can lead to emergent behaviors, that is, the equilibrium configurations of a large-scale complex channel network may not be a simple combination of individual bifurcations (Gao et al., 2023; Kleinhans et al., 2012; Ragno et al., 2021, 2022a, 2022b; Salter et al., 2020).

Recently, morphological equilibria of simple tree-like channel networks, that is, an initial channel splits into two branches at an upstream bifurcation and each branch further splits into two more branches at the two downstream bifurcations, have been explored (Ragno et al., 2022b; Salter et al., 2020). These studies have demonstrated emergent behaviors in such channel networks driven by downstream controls such as tides or net-deposition. Specifically, Salter et al. (2020) showed that aperiodic yet bounded chaotic water and sediment partitioning arose in such channel networks with net-deposition, while periodic partitioning pattern emerged in a single channel bifurcation (Salter et al., 2018). More recently, Ragno et al. (2022b) showed that small tides can either mitigate or augment the asymmetric water and sediment partitioning at the upstream bifurcation in a tree-like channel network, contrasting with their consistent role in mitigating asymmetric partitioning of a single bifurcation (Ragno et al., 2020). Nonetheless, the above emergent behaviors in tree-like channel networks are largely driven by downstream boundary conditions such as tides or net-deposition caused by relative sea level rise. In this study, we investigated whether internal dynamics resulted from a shortcut channel (termed "connecting channel" hereinafter) connecting two downstream branches (Figure 1) can lead to an emergent behavior, such as dynamic water partitioning at channel bifurcations of the network, under constant boundary conditions and without net-deposition.

Specifically, we examined a simple and common channel network of the "bifurcation-connecting channel" unit (hereinafter termed the B-C network) in river deltas and braided rivers (Figure 1). While Gao et al. (2023) have shown that the connecting channel can significantly modulate the water and sediment partitioning in the channel network, its morphodynamics are yet unexplored. In this simple yet representative topological structure of deltaic channel networks, we conducted a series of numerical simulations using a reduced-complexity morphodynamic model with a wider parameter space than Gao et al. (2023). We observed and reported internal dynamics between the upstream water partitioning and downstream water level via a connecting channel that led to periodic water

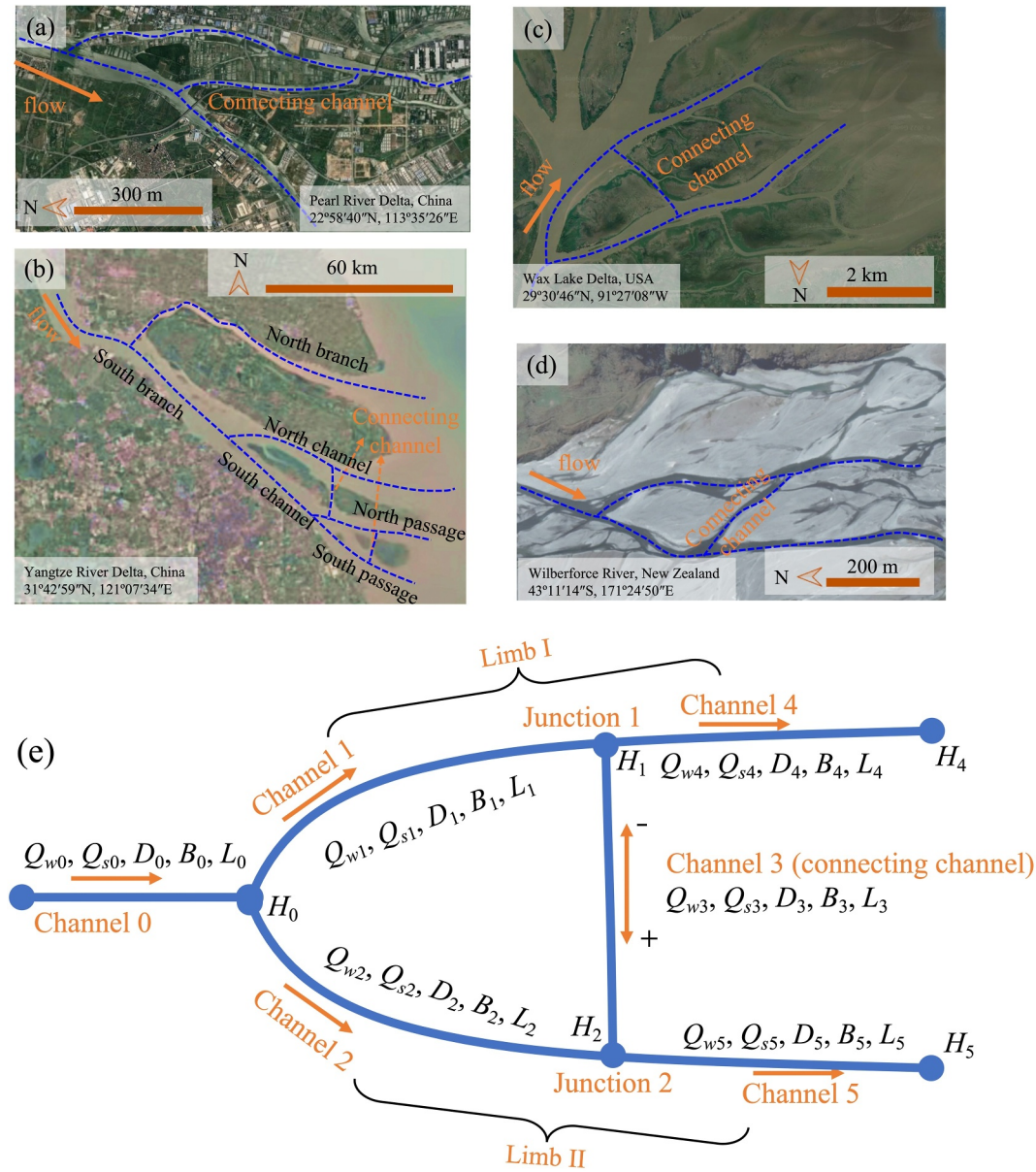

Figure 1. Panels (a–d) are examples of the "bifurcation-connecting channel" unit in river deltas and braided river. Panel (e) shows the schematic channel network of the "bifurcation-connecting channel" unit (the B-C network), with the orange arrows indicating the assumed flow directions. Q_{wi}, Q_{si}, D_i, B_i and L_i are the discharges, sediment loads, water depths, channel widths and lengths, respectively, of each channel ($i = 0 – 5$ is the channel number). H_j are the water levels at the downstream ends of each channel except the connecting channel ($j = 0 – 2$ and $4 – 5$). For Channel 3, the positive direction is from Junction 1 to Junction 2, while the orange arrows indicate the positive direction of other channels. Satellite images are from Google Earth (https://earth.google.com/).

partitioning in the channel network under constant boundary conditions. A better understanding of these feedbacks and behaviors can help inform and predict the equilibrium configurations of channel networks.

In the following, the basic assumptions, governing equations and modeling parameters for the reduced-complexity morphodynamic model of the B-C network are provided in Section 2 (see also Gao (2023)). Section 3.1 documents the emergence of different equilibrium configurations of the B-C network, and Section 3.2 illustrates the mechanisms leading to the different equilibrium configurations. The comparisons of the results with previous studies and field observations are conducted in Section 3.3, whereas the implications for the evolution

and restoration of deltaic channel networks under human interventions are discussed in Section 3.4. Finally, the main conclusions are drawn in Section 4.

2. Methodology

2.1. Governing Equations

As shown in Figure 1e, the initial river channel (Channel 0) first splits into two downstream limbs, that is, Limb I (including Channel 1 and Channel 4) and Limb II (including Channel 2 and Channel 5). A connecting channel (Channel 3) further links the two limbs at their midways (denoted as Junction 1 and Junction 2) by cutting through floodplains or deltaic islands (Gao et al., 2023; Nanson & Knighton, 1996; Salter & Lamb, 2022; Swinkels et al., 2009; Wang et al., 2015). Essentially, the studied channel network, that is, the B-C network, consists of an upstream primary bifurcation and two downstream junctions (junctions 1 and 2) which can alternate between bifurcation and confluence depending on the flow direction in Channel 3. In the following, we introduce the basic assumptions and governing equations for the morphological evolution of the B-C network.

Following previous studies (Schielen & Blom, 2018; Wang et al., 1995), we adopted the assumption of normal flow conditions and the assumption of $\Delta D_i = -\Delta\eta_i$ (where $\Delta\eta_i$ and ΔD_i are changes in branch-averaged bed elevation and water depth, respectively) in each channel. The above assumptions were adopted to reduce computational costs, which are valid when the changes in water levels are relatively small and negligible (see Figure S2 in Supporting Information S1) and when the wave of bed elevation change migrates relatively fast in the channel or the channel is relatively short (Schielen & Blom, 2018). Therefore, the changes in branch-averaged water depths in each channel based on mass conservation of sediment yield

$$\frac{\mathrm{d}D_i}{\mathrm{d}t} = \frac{Q_{sei} - Q_{si}}{(1-p)\,B_i L_i} \tag{1}$$

where D_i is the branch-averaged water depth, Q_{si} (m^3/s) and Q_{sei} (m^3/s) represent the sediment supply from the upstream boundary and the sediment transport capacity of Channel i, and p (=0.4) is bed porosity. The subscript i is the channel number (see Figure 1e). The nondimensional time is defined as $t_* = t/(\alpha B_0^2 D_0(1-p)/Q_{s0})$.

The adoption of Equation 1 thus represents a zero-dimensional modeling framework. Nonetheless, further simulations with longer channels using a one-dimensional model solving the Saint-Venant equations for hydrodynamics do not change the conclusions of this study, that is, the emergence of different equilibrium configurations of the channel network (see the detailed comparisons between the zero- and one-dimensional simulations in Figure S3–S8 in Supporting Information S1).

To solve Equation 1, the following equations are further provided. The mass conservation of water and sediment at a bifurcation or confluence reads:

$$\sum Q_{w,u} = \sum Q_{w,d} \tag{2}$$

$$\sum Q_{s,u} = \sum Q_{s,d} \tag{3}$$

where $Q_{w,u}$ (m^3/s) and $Q_{s,d}$ (m^3/s) are the upstream coming river discharge and sediment load of a bifurcation/confluence, respectively; $Q_{w,d}$ (m^3/s) and $Q_{s,d}$ (m^3/s) are the discharges and sediment leaving the bifurcation/confluence through the downstream channel(s), respectively. Notably, we did not specify the channel number i in Equations 2 and 3 since junctions 1 and 2 can be either a bifurcation or confluence depending on the flow direction in Channel 3.

Assuming normal flow conditions, the discharge in each river channel Q_{wi} is:

$$Q_{wi} = B_i C_i D_i^{3/2} S_i^{1/2} \tag{4}$$

where B_i (m) is the channel width, C_i ($m^{1/2}/s$) is the Chezy coefficient, D_i (m) is the water depth, S_i is the water surface slope. Water surface slope S_i reads:

$$S_i = \frac{H_{iu} - H_{id}}{L_i} \tag{5}$$

where H_{iu} and H_{id} are the water level at the upstream and downstream boundaries of river channel i, and L_i is the length of river channel i. Notably, the water levels at the bifurcation or confluence is assumed to be the same for all the channels connected (Bolla Pittaluga et al., 2003; van Denderen et al., 2018). However, Ragno et al. (2021) suggested that the water level of the dominant branch connected to a confluence tends to be higher than the subordinate branch, which thus stabilizes the upstream bifurcation; these effects are not yet considered in this study.

In this study we focused on sand-bed rivers and adopted the Engelund-Hansen formula (Engelund & Hansen, 1967) for sediment transport capacity in each river channel, which reads:

$$Q_{sei} = B_i \sqrt{Rgd_{50}{}^3} m\theta_i^n \tag{6}$$

where R (=1.65) is the submerged specific density of sediment, g (m/s^2) is gravitational acceleration, d_{50} (m) is the median sediment grain size, and the coefficients $m = 0.05$ C^2/g and $n = 2.5$. The Shields stress of each river channel θ_i can be written as:

$$\theta_i = \frac{1}{Rd_{50}} \left(\frac{Q_{wi}}{B_i C_i D_i} \right)^2 \tag{7}$$

At the channel bifurcations, we adopted the nodal-point relation of Bolla Pittaluga et al. (2003) for the sediment partitioning at the bifurcations in this study, which can be written as:

$$\frac{Q_{s,d1}}{Q_{s,d2}} = \frac{Q_{w,d1} + \frac{2\alpha r (D_{d1} - D_{d2})}{\sqrt{\theta_u} B_u} Q_{w,u}}{Q_{w,d2} - \frac{2\alpha r (D_{d1} - D_{d2})}{\sqrt{\theta_u} B_u} Q_{w,u}} \tag{8}$$

where α is the ratio between the length of the river section allowing transverse sediment exchange and the upstream channel width, r is a coefficient of transverse sediment transport ranging from 0.3 to 1 (Ikeda et al., 1981; Talmon et al., 1995), and the subscripts u and d for each variable indicate the upstream and downstream channels connected to a bifurcation, respectively. Notably, we used the subscripts u and d instead of the channel number i, since Junctions 1 and 2 can alternate between bifurcation and confluence depending on the flow direction in Channel 3. Therefore, Equation 8 using the subscripts u and d is more convenient and straightforward for this study. See the in Supporting Information S1 for the detailed derivation of Equation 8. Equation 1 thus can be solved by incorporating Equations 2–8 (see Gao (2023)).

2.2. Parameter Space

We simulated the morphological evolution of the B-C network given different Shields stress θ_0 and aspect ratio β_0 (=B_0/D_0) of the upstream river channel, widely ranging from 0.05 to 5 and from 5 to 40, respectively, in this study. θ_0 and β_0 are two critical parameters determining the equilibrium configurations of a single bifurcation (Bolla Pittaluga et al., 2003, 2015). The initial perturbations in Limb I of the channel network (i.e., Channel 1 and Channel 4) were implemented upon a symmetric single upstream primary bifurcation. Specifically, we changed both initial D_1 and D_4 to different proportions, that is, [0.5, 0.7, 0.9, 0.99999], of D_2 and D_5, respectively. Initial D_3 was set to $0.3D_1$ for all simulation scenarios since the connecting channel is relatively shallow as compared with the main branches (Limbs I and II). The other modeling parameters and boundary conditions are listed as follows.

- Channel length: $L_1 = L_2 = L_3 = L_4 = L_5 = 1$ km
- Channel width: $B_1 = B_2 = B_3 = B_4 = B_5 = 50$ m, $B_0 = 100$ m
- The empirical coefficients of transverse sediment transport in the nodal-point relation are: $\alpha = 3$ and $r = 0.5$
- Chezy coefficient: $C_i = 40$ m$^{1/2}$/s

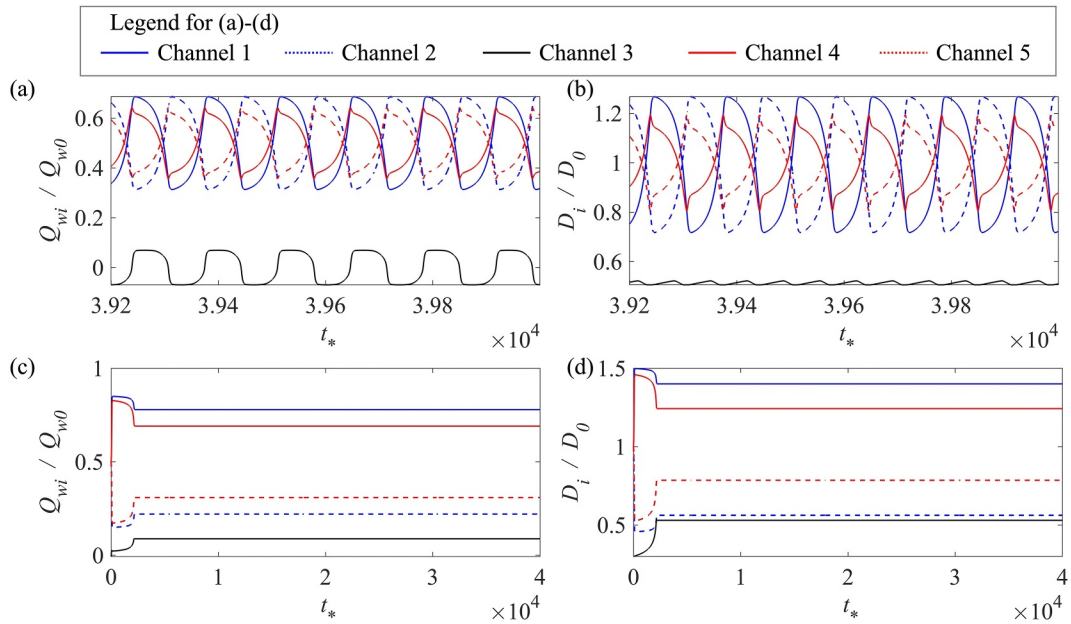

Figure 2. The normalized discharges and water depths over time in each channel when attaining a periodic solution (a–b), and steady-state solution (c–d). Shields stress of the upstream river channel $\theta_0 = 2$ for panels (a–b) and $\theta_0 = 3$ for panels (c–d), and aspect ratio of the upstream river channel $\beta_0 = 20$ for panels (a–d). Q_{w0} and D_0 are the river discharge and water depth, respectively, in the upstream channel, and i (=1 – 5) is the channel number.

- Upstream river discharge: $Q_{w0} = 400$ m^3/s
- Water levels at the outlets: $H_4 = H_5 = 0$ m, as we do not consider tides, waves, and relative sea level rise in this study
- Sediment load Q_{s0} and sediment grain size d_{50} can be calculated using Equations 6 and 7 given a specific value of θ_0 and β_0

In this study, discharge asymmetry ΔQ was adopted to quantify river discharge partitioning at the upstream primary bifurcation:

$$\Delta Q = \frac{Q_{w1} - Q_{w2}}{Q_{w0}} \tag{9}$$

ΔQ ranges from −1 to 1, where $\Delta Q = 0$ represents a symmetric discharge partitioning, and $\Delta Q = \pm 1$ represents the closure of one of the downstream branches, that is, one of the branches takes all the river discharge.

3. Results and Discussions

3.1. Different Equilibrium Regimes in Relation to Shields Stress and Channel Aspect Ratio

As shown in Figure 2, we found that the discharges and water depths in each channel of the B-C network have two distinctive behaviors depending on the Shields stress θ_0 (or channel aspect ratio β_0). Specifically, the discharges and water depths either vary periodically over time (hereinafter periodic solution of the channel network, Figures 2a and 2b) or eventually attain a steady state (hereinafter steady-state solution of the channel network, Figures 2c and 2d). For the periodic solution, discharges and water depths in Channels 1 and 2 (as well as Channels 4 and 5) oscillate around a symmetric configuration, with alternative shifting of the dominant branch. Furthermore, the discharge in Channel 3 oscillates in both magnitude and directions, implying the shifting of bifurcation and confluence for Junctions 1 and 2. Notably, the magnitude of oscillatory water depth in Channel 3 is relatively small compared with those of Channels 1 – 2 and 4 – 5, presumably due to the relatively low discharge and hence smaller bed level change in the connecting channel (Figure 2a).

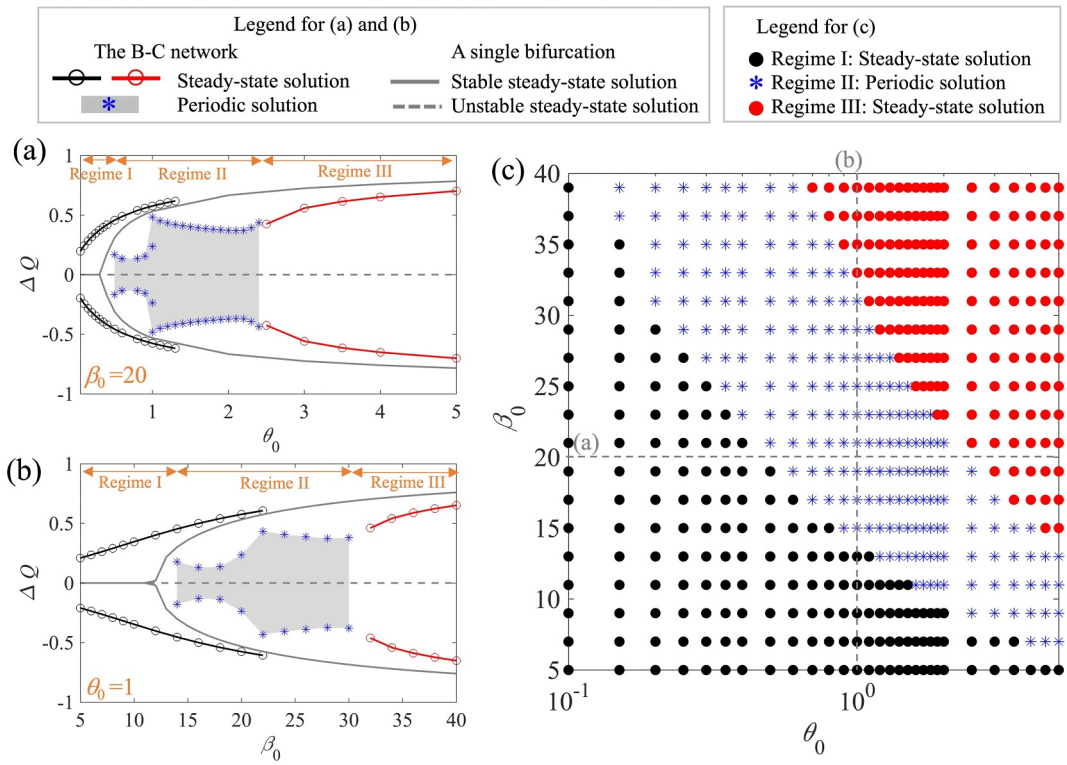

Figure 3. Equilibrium configurations of the B-C network and a single bifurcation in relation to (a) Shields stress θ_0 and (b) aspect ratio β_0 in the upstream channel. Panel (c) shows the different regimes in the parameter space of θ_0 versus β_0. ΔQ is the discharge asymmetry of the upstream bifurcation. The shaded area with blue asterisks in panels (a–b) indicates the oscillatory range of ΔQ when attaining the periodic solution. The B-C network refers to the channel network of the "bifurcation-connecting channel".

In the following, we further illustrate the emergence of the periodic and steady-state solutions of the B-C network related to Shields stress θ_0 and channel aspect ratio β_0. Notably, we focused on the partitioning of river discharge at the upstream bifurcation in the B-C network (see Figure 1e), which facilitates the comparisons with the results of a single bifurcation in previous studies (Bolla Pittaluga et al., 2015).

When the connecting channel is absent, the B-C network degenerates to a single bifurcation. In such cases, the single upstream bifurcation attains a steady-state solution with either symmetric or asymmetric water partitioning with relatively low and high Shields stress θ_0 (or channel aspect ratio β_0), respectively (gray lines in Figures 3a and 3b). These results are consistent with previous studies (Bolla Pittaluga et al., 2015), which suggests that the bifurcation instability increases with increasing θ_0 (or β_0) in sand-bed rivers. Notably, the equilibrium configurations of a single bifurcation are trivial solutions for the B-C network by assuming the connecting channel is inactive and conveys no discharge. Also, such solutions are delicate as a small disturbance in the two branches will re-activate the dormant connecting channel. Therefore, the equilibrium configurations of a single upstream bifurcation are considered as unstable equilibria for the B-C network in this study.

As shown in Figure 3, the equilibrium configurations of the B-C network with the existence of the connecting channel can be dictated by three regimes related to Shields stress θ_0 (or channel aspect ratio β_0):

Regime I: With relatively low θ_0 (or β_0), the channel network eventually attains a steady-state solution with higher discharge asymmetry at the upstream bifurcation than a single bifurcation (see the black lines in Figures 3a and 3b).

Regime II: With moderate θ_0 (or β_0), the channel network attains a periodic solution with smaller discharge asymmetry at the upstream bifurcation than a single bifurcation (see the shaded area with blue asterisks in Figures 3a and 3b).

Regime III: With relatively high θ_0 (or β_0), the channel network eventually evolves to a steady-state solution with smaller discharge asymmetry at the upstream bifurcation than a single bifurcation (see the red lines in Figures 3a and 3b).

Notably, the shaded area in Figures 3a and 3b indicates the oscillatory ranges of ΔQ when attaining the periodic solution. Furthermore, we also observed that the periodic solution could coexist with the steady-state solution in regime II with relatively low θ_0 (or β_0) (Figures 3a and 3b). In such cases, whether the channel network attains the steady-state or periodic solution in regime II primarily depends on the initial difference in the water depths of the two limbs, which is discussed in the following Section. Nonetheless, in this study the criterion for attaining regime II is the existence of the periodic solution, therefore the parameter space for the coexistence of the two types of solutions is not shown in Figure 3c.

3.2. Mechanisms Leading to Different Equilibrium Regimes

The above equilibrium regimes in the B-C network (Figure 3) essentially result from the dynamic interactions between the bifurcation instability and the downstream water surface slope advantage (i.e., the slope difference between Channels 1 and 2, and hereinafter termed slope advantage for simplicity). A slope advantage in Channel 1 develops when $H_1 < H_2$, whereas Channel 2 attains a slope advantage with $H_1 > H_2$ (see Figures 4c–4f). In this study, the bifurcation instability refers to the nature of the bifurcation to develop an asymmetric configuration (Bolla Pittaluga et al., 2015).

Essentially, the periodic solution arises from the dynamic interactions between the bifurcation instability and the downstream water surface slope advantage modulated by the connecting channel. Specifically, the bifurcation instability leads to the development of a slope advantage in the subordinate branch, which is possible with the existence of the connecting channel. The developed slope advantage in turn changes the bifurcation instability that turns the subordinate branch to the dominant one.

3.2.1. The General Interactions Between Bifurcation Instability and Slope Advantage

When the connecting channel is absent (i.e., $D_3 = 0$) and the B-C network reduces to a single bifurcation, the water surface slopes in the two limbs are dictated by the water levels at the upstream bifurcation node and the two outlets (see Figures 4a, 4b, and 4g). In contrast, the existence of the connecting channel provides a degree of freedom for the adjustment of water levels at Junctions 1 and 2 (i.e., H_1 and H_2) associated with the setup of the water surface slope (and hence the discharge) in the connecting channel (Channel 3). The changing discharges in Channels 1 and 2 (as well as the sediment loads) driven by bifurcation instability can thus lead to different water surface slopes between Channels 1 and 2 through the changing H_1 and H_2 (Figures 4c–4f). The changing H_1 and H_2 are a response to the morphological changes, that is, a disbalance between the sediment supply from the upstream node of each channel and its sediment transport capacity causes sedimentation or erosion and hence the changed discharge in the channel. The changed discharge can further alter the slope (as well as water depth) to counteract the disbalance. Specifically, under bifurcation instability, the deepening riverbed of Channel 1 or 2 due to sediment deficit tends to be associated with a decreasing water surface slope, that is, the increasing water level of H_1 or H_2, to reduce the sediment transport capacity to match the sediment supply, and vice versa. Notably, the changing H_1 and H_2 will further affect the bifurcation instability (Figure 5).

The changing H_1 and H_2 are then maintained by the different discharges between Channels 1 and 4 of Limb I (also Channels 2 and 5 of Limb II) modulated by the connecting channel as demonstrated below (see also Figure 4g). Assuming $H_1 > H_2$ (e.g., Figure 4f), the connecting channel thus drains discharge from Limb I to Limb II ($Q_{w3} > 0$), which leads to $Q_{w1} > Q_{w4}$ and $Q_{w2} < Q_{w5}$. $Q_{w1} > Q_{w4}$ will result in an increasing water surface slope from Channel 1 to Channel 2 along Limb I, that is, $S_1 < S_4$, whereas $Q_{w2} < Q_{w5}$ would lead to a decreasing water surface slope from Channel 4 to Channel 5 along Limb II, that is, $S_2 > S_5$ (Sinha & Parker, 1996; Wang et al., 2008). $S_1 < S_4$ and $S_2 > S_5$ in turn ensure the maintaining of $H_1 > H_2$, given the same water levels at the upstream bifurcation node (H_0) and the two outlets (H_4 and H_5). The above mechanisms for the development of slope advantage are summarized schematically in Figure 4g.

Furthermore, the water levels of each channel are constant over time when attaining a steady-state solution (Figures 4c and 4d), while the water levels of each channel keep changing over time (associated with different discharges) when attaining the periodic solution (Figures 4e and 4f). Notably, the water surfaces in Figure 4 are

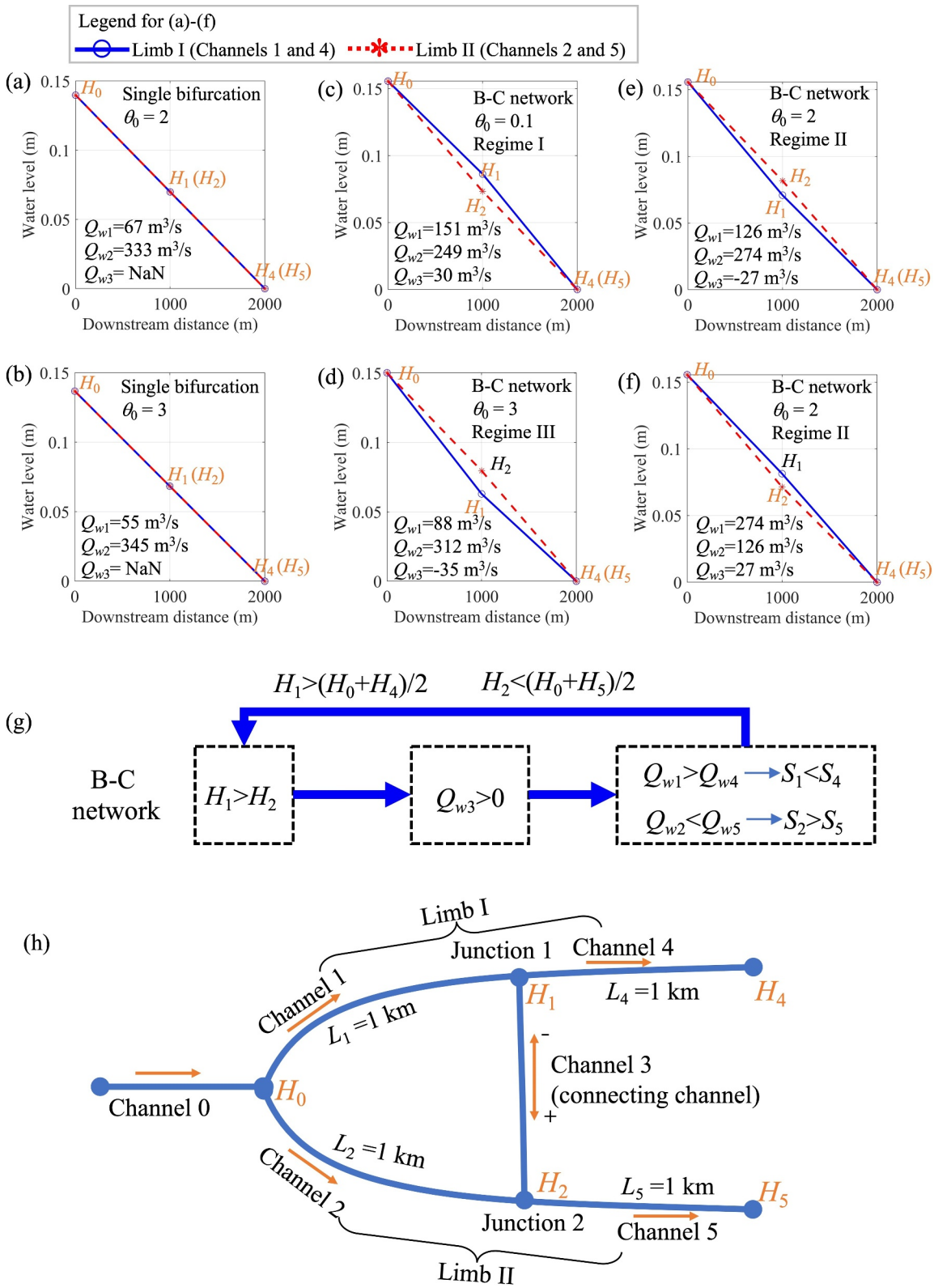

Figure 4. The water levels for (a–b) a single bifurcation and (c–f) the B-C network, with different Shields stress θ_0. Panel (g) is a schematic of the effects of connecting channel on the development of the slope advantage. Panel (h) depicts the nodes and channels of the B-C network, showing the definition of water levels and the channel number. Channel aspect ratio $\beta_0 = 20$ for the plotted scenarios in panels (a–f). Notably, Channel 3 (i.e., the connecting channel) is absent for a single bifurcation (panels a and b). The B-C network refers to the channel network of the "bifurcation-connecting channel".

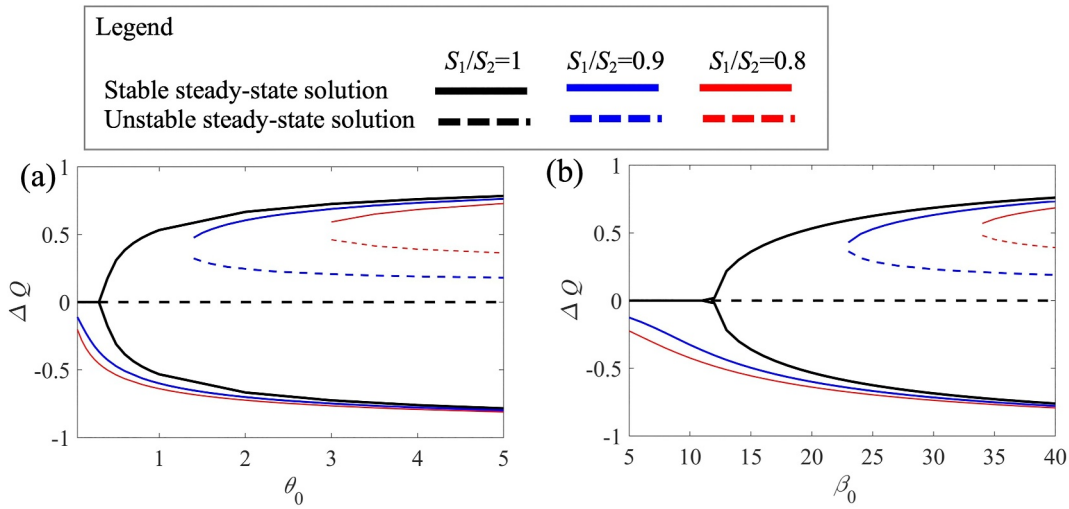

Figure 5. Equilibrium configurations of a single bifurcation in relation to (a) Shields stress θ_0 and (b) channel aspect ratio β_0 with different slope advantages between the two branches.

delineated by the water levels in the upstream and downstream ends of each channel, since we adopted the zero-dimensional model in this study. Therefore, the water surface slopes are the branch-averaged values (see Equation 5). Moreover, in this study we focus on the different water surface slopes between Channels 1 and 2, since they are directly linked to the primary upstream bifurcation.

In the following, we further illustrate how the different water surface slopes between Channels 1 and 2 (Figures 4c–4f) affect the equilibrium configuration of the primary upstream bifurcation. As shown in Figures 5a and 5b, the slope advantage tends to more significantly affect the equilibrium configurations of a single bifurcation with relatively low Shields stress θ_0 or channel aspect ratio β_0 (see also Figure S9 in Supporting Information S1). Specifically, the bifurcation can only attain one stable asymmetric steady-state solution at relatively low Shields stress θ_0 or channel aspect ratio β_0, while the stable steady-state solutions are close to those without slope advantage at relatively high Shields stress θ_0 or channel aspect ratio β_0. The effects of slope advantage on the equilibrium configurations of a single bifurcation are consistent with Redolfi et al. (2019). Notably, in this study the slope advantage in Figures 5a and 5b were attained by imposing different water levels at the downstream ends of the two branches (Channels 1 and 2) (Figures 4c–4f), while the slope advantage in Redolfi et al. (2019) is due to the different lengths between the two branches.

As demonstrated above, in the B-C network the changing discharges driven by bifurcation instability can lead to a slope advantage between Channels 1 and 2 (Figures 4c–4f), the slope advantage can in turn affect the bifurcation instability (Figure 5). In the following, we demonstrated how the interactions between bifurcation instability and slope advantage lead to different equilibrium configurations in the B-C network.

3.2.2. Mechanisms Leading to the Periodic Solution in Regime II

For the periodic solution in regime II with moderate Shields stress θ_0 (or channel aspect ratio β_0), an asymmetric river discharge partitioning is first initiated due to the bifurcation instability (Bolla Pittaluga et al., 2015), leading to a dominant branch (say Channel 2) and a subordinate branch (say Channel 1) conveying more and less discharges, respectively ($t_0 - t_1$ in Figure 6a). The bifurcation instability leads to a continuous erosion in Channel 2, that is, a deepening stage, since the sediment transport capacity is larger than the sediment supply to Channel 2. The deepening stage is associated with a decreasing water surface slope, that is, an increasing H_2, since the channel tends to adjust its water surface slope to match the sediment transport capacity with the sediment supply. In contrast, Channel 1 undergoes continuous siltation, that is, a shallowing stage, which is associated with an increasing water surface slope, that is, a decreasing H_1. The increasing H_2 and decreasing H_1 are further maintained by the discharges modulated by the connecting channel, leading to $Q_{w1} < Q_{w4}$ and $Q_{w2} > Q_{w5}$ (see Figure 4g). Subsequently, the slope advantage developed in Channel 1 suppresses the further development of the asymmetric river discharge partitioning, and finally changes the bifurcation instability that further drives Channel

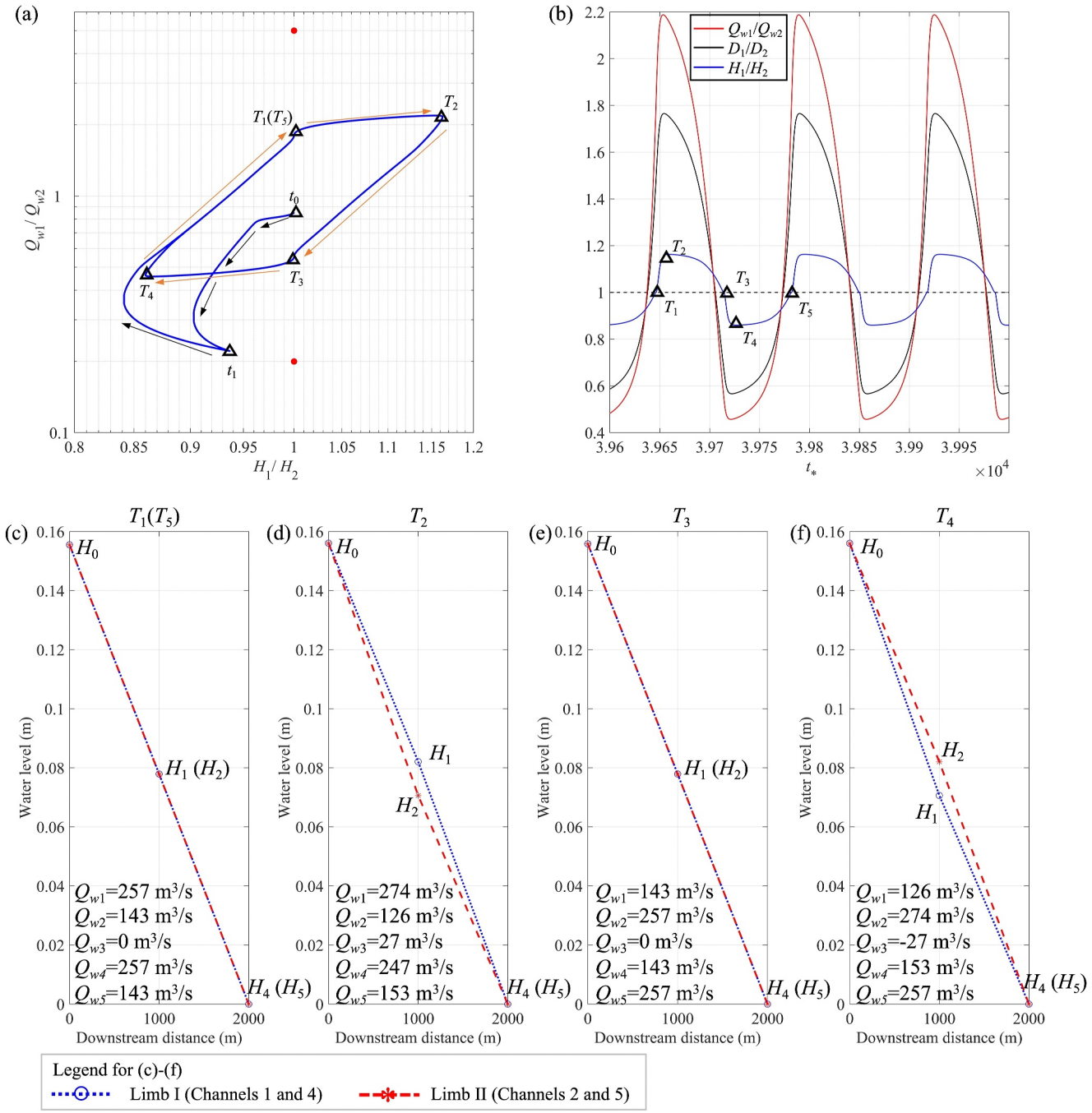

Figure 6. (a) The trajectories of H_1/H_2 versus Q_{w1}/Q_{w2} in regime II with Shields stress $\theta_0 = 2$ and channel aspect ratio $\beta_0 = 20$ for the B-C network (blue line). The red dots in panel (a) are the equilibrium configurations of the corresponding single bifurcation. t_0, t_1 and $T_1 - T_5$ are representative time instants. Panel (b) is the associated time series of river discharge ratio Q_{w1}/Q_{w2}, water depth ratio D_1/D_2 and water level ratio H_1/H_2. Panels (c–f) show the water levels in Limbs I and II associated with different discharges in Channels 1 and 2 at time instants T_1-T_5. The B-C network refers to the channel network of the "bifurcation-connecting channel".

1 to become the dominant branch ($t_1 - T_1$ in Figure 6a). The above processes thus create a periodic water partitioning in the channel network (the cycles indicated by the orange arrows in Figure 6a). We further demonstrated a full cycle of the periodic solution at representative time instants, that is, $T_1 - T_5$, in Figures 6b–6f (see also Figure S10 in Supporting Information S1) as follows.

1. **From T_1 to T_2**: The bifurcation instability drives the continuous deepening of Channel 1 and shallowing of Channel 2. While the continuous deepening of Channel 1 is associated with a decreasing water surface slope,

the shallowing of Channel 2 is associated with an increasing water surface slope. Furthermore, the slope advantage developed in Channel 2 from T_1 to T_2 is associated with the discharges modulated by the connecting channel ($Q_{w3} > 0$), that is, $Q_{w1} > Q_{w4}$ and $Q_{w2} < Q_{w5}$ (Figures 6c and 6d).

2. **From T_2 to T_3**: The continuous development of the slope advantage in Channel 2 finally changes the bifurcation instability at T_2 (see Figure 5), leading to the subsequent deepening of Channel 2 and shallowing of Channel 1. The deepening and shallowing of Channels 2 and 1 are associated with decreasing and increasing water surface slopes, respectively, which is also maintained by the decreasing discharge in the connecting channel, that is, Q_{w3} gradually decreases to 0 at T_3. Finally, the slope advantage shifts to Channel 1 after T_3 (Figures 6d and 6e).
3. **From T_3 to T_4**: Although the bifurcation instability still drives the continuous deepening of Channel 2 and shallowing of Channel 1, the slope advantage in Channel 1 starts to suppress the continuous deepening of Channel 2 and shallowing of Channel 1. During this stage, the connecting channel drains discharge from Limb II to Limb I, that is, $Q_{w3} < 0$, leading to $Q_{w1} < Q_{w4}$ and $Q_{w2} > Q_{w5}$ (Figures 6e and 6f). Finally, the slope advantage in Channel 1 changes the bifurcation instability at T_4 (see also Figure 5).
4. **From T_4 to T_5**: The changed bifurcation instability starts to drive the subsequent deepening of Channel 1 and shallowing of Channel 2, associated with a decreasing and increasing water surface slope in Channels 1 and 2, respectively, that is, a decreasing S_1 and increasing S_2. The decreasing S_1 and increasing S_2 are also maintained by the decreasing discharge drained from Limb II to Limb I through the connecting channel, that is, Q_{w3} gradually increases from -27 to 0 m^3/s at T_5. Finally, the slope advantage shifts to Channel 2 after T_5 (Figures 6a and 6f).

To demonstrate the effects of the modulated discharges by the connecting channel on the development of the periodic solution, we further conducted additional simulations with different fixed bed levels (and hence roughly fixed water depths) in the connecting channel (Figure 7, see also Figure S11 in Supporting Information S1 for the 1D simulation scenarios). The channel network tends to attain a steady-state solution when the water depth of the connecting channel is fixed at a relatively low value (red dots in Figure 7a). In such cases, the flow through the connecting channel is relatively low (red dots in Figure 7b), translating to a lower capacity of the connecting channel to modulate the discharge distribution in the entire channel network. In contrast, a relatively large water depth in the connecting channel, allowing a relatively high flow, tends to lead to a periodic solution (blue asterisks in Figures 7a and 7b). Notably, the critical water depth and associated discharge in the connecting channel above which the channel network attains a periodic solution are generally consistent with those derived from simulations with a morphologically active connecting channel (dashed lines in Figures 7a and 7b). Notably, we also observed that the periodic solution could coexist with steady-state solution in regime II. The steady-state solution in regime II is attained when the initial water depth difference between the two limbs is sufficiently large such that the slope advantage is unable to shift the dominant branch. Therefore, in reality, the water depths when sufficiently altered by dredging activities (Jeuken & Wang, 2010; Riquier et al., 2017) could lead to the transition from periodic solution to steady-state solution (Figure 8).

3.2.3. Mechanisms Leading to the Steady-State Solution in Regimes I and III

In the following, we further demonstrated the mechanism leading to the steady-state solution of the B-C network with relatively high and low Shields stress θ_0 (or channel aspect ratio β_0), that is, regimes III and I (Figure 3). When the Shields stress θ_0 (or channel aspect ratio β_0) is relatively high (regime III), the strong bifurcation instability tends to drive the upstream bifurcation toward an asymmetric water partitioning ($t_0 - t_1$ of the blue lines in Figures 9a and 9b). Therefore, the trajectory of D_1 versus D_2 for the B-C network largely overlaps with that of a single bifurcation during $t_0 - t_1$ (the red dashed line in Figure 9b). During this stage, the continuous erosion in Channel 2 leads to an increasing H_2, while the continuous siltation in Channel 1 leads to a decreasing H_1. In such cases, the connecting channel drains discharge from Limb II to Limb I, that is, $Q_{w3} < 0$, leading to $Q_{w1} < Q_{w4}$ and $Q_{w2} > Q_{w5}$ that maintain the slope advantage in Channel 1 (see also Figure 4d). Further, the developed slope advantage in Channel 1 suppresses the development of the asymmetric water partitioning but fails to result in the shifting of the dominant branches ($t_1 - t_2$ of the blue lines in Figures 9a and 9b). As a result, the upstream bifurcation attains a steady-state solution with a reduced asymmetric water partitioning and with the connecting channel draining discharge from Limb II (the dominant branch) to Limb I (the subordinate branch). This is also

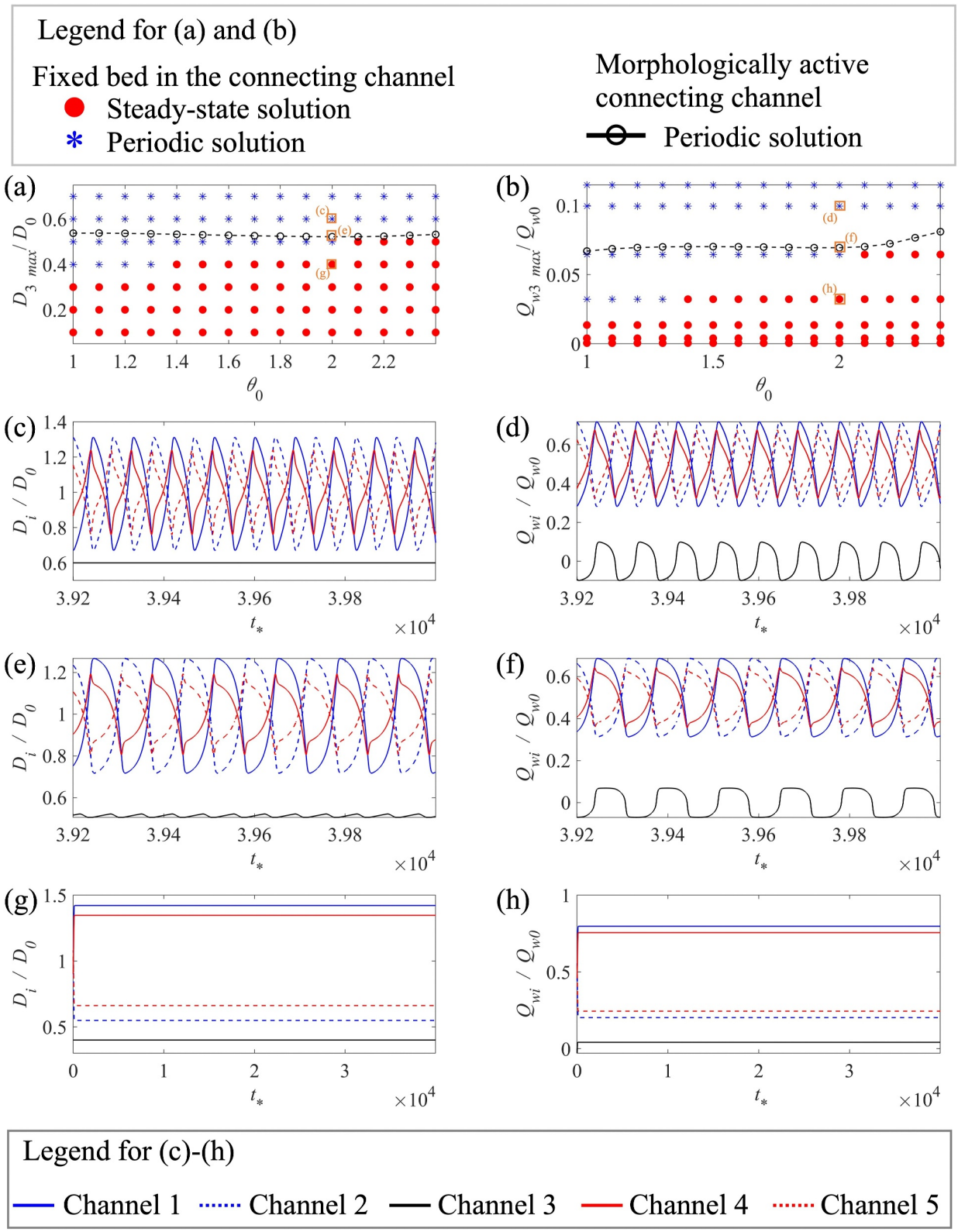

Figure 7. Panel (a) shows the equilibrium configurations of the B-C network with different Shields stress θ_0 and fixed water depth in the connecting channel D_{3max} relative to the water depth in the upstream channel D_0, with panel (b) showing the associated parameter space of Shields stress θ_0 versus maximum absolute value of discharge in the connecting channel Q_{w3max}. Channel aspect ratio $\beta_0 = 20$ for the plotted scenarios. Panels (c–h) are the normalized water depths D_i/D_0 and discharges Q_{wi}/Q_{w0} over time in each channel for the scenarios indicated in panels (a) and (b).

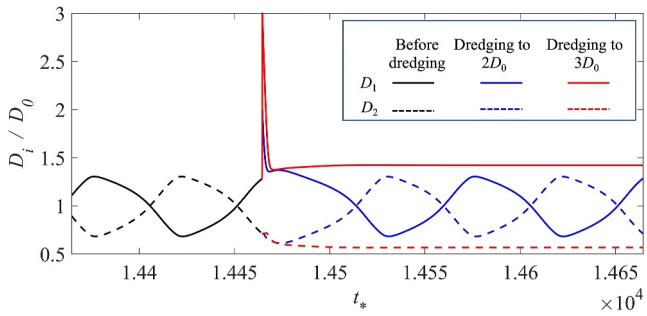

Figure 8. Evolution of water depths in Channel 1 (D_1) and Channel 2 (D_2) of the B-C network subject to different dredging depths in Limb I. The Shields stress $\theta_0 = 1.2$ and channel aspect ratio $\beta_0 = 20$ for the plotted scenarios. D_0 is the water depth in the upstream channel, and i (=1 or 2) is the channel number. The B-C network refers to the channel network of the "bifurcation-connecting channel".

consistent with Figure 5, which shows that the slope advantage has lesser effects on the equilibrium configuration of the upstream bifurcation with increasing Shields stress θ_0 (or channel aspect ratio β_0).

Finally, for regime I with relatively low Shields stress θ_0 (or channel aspect ratio β_0), the trajectory of D_1 versus D_2 for the B-C network (the blue line in Figure 9d) largely overlaps with that of a single bifurcation (the red dashed line in Figure 9d) during $t_0 - t_1$. When approaching to t_1, $H_1 > H_2$ develops due to the greater erosion in Channel 1 than that in Channel 2 (Figure 9d), leading to a slope advantage in Channel 2. In such cases, the connecting channel drains discharge from Limb I to Limb II, that is, $Q_{w3} > 0$, leading to $Q_{w1} > Q_{w4}$ and $Q_{w2} < Q_{w5}$ that maintain the development of slope advantage in Channel 2 (see also Figure 4c). Later, the developed slope advantage in Channel 2 is dominant in determining the water partitioning at the upstream bifurcation ($t_1 - t_2$ of the blue lines in Figures 9c and 9d), leading to continuously increasing discharge in Channel 2. At the same time, the connecting channel drains discharge from Limb I (the subordinate branch) to Limb II (the dominant branch) due to $H_1 > H_2$. In such cases, the slope advantage in Channel 2 results in an increased asymmetry of the water

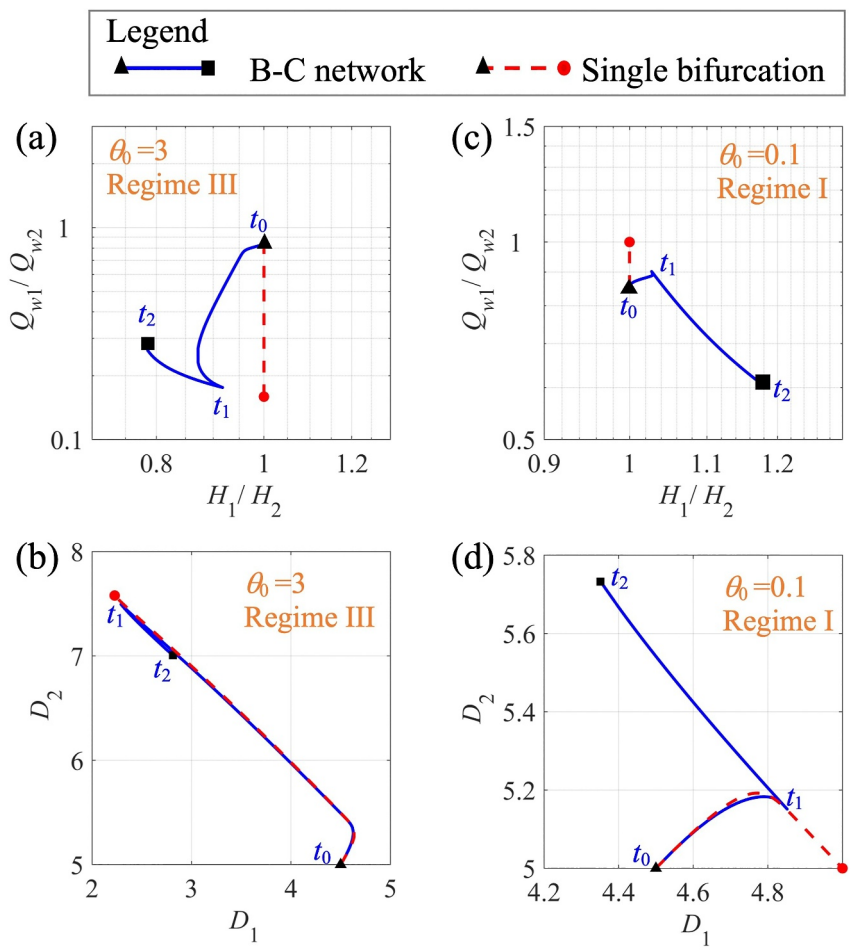

Figure 9. The trajectories of H_1/H_2 versus Q_{w1}/Q_{w2} and D_1 versus D_2 for representative scenarios of regime III with Shields stress $\theta_0 = 3$ (a–b) and regime I with Shields stress $\theta_0 = 0.1$ (c–d). t_0, t_1 and t_2 are representative time instants. Channel aspect ratio $\beta_0 = 20$ for the plotted scenarios. The B-C network refers to the channel network of the "bifurcation-connecting channel".

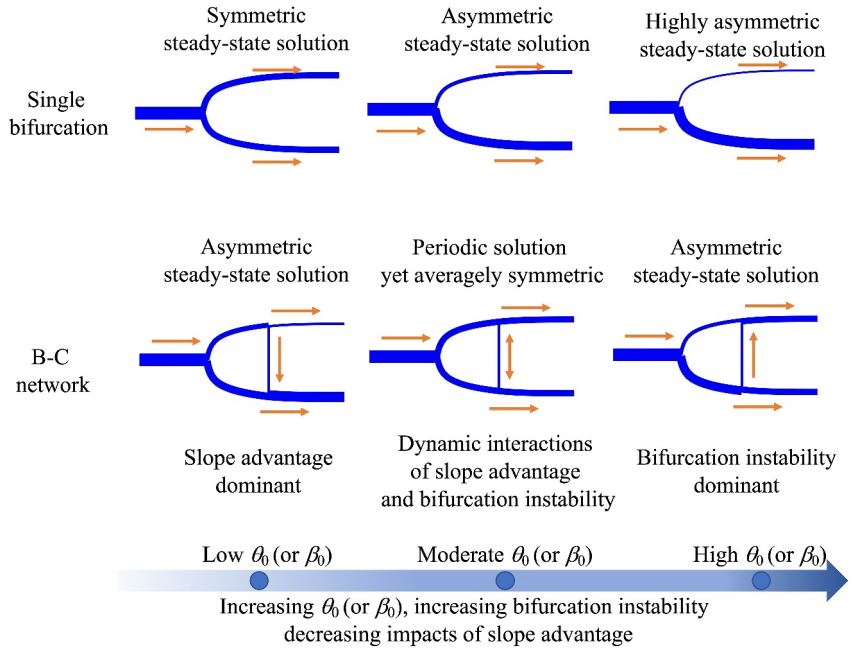

Figure 10. The schematics showing the different equilibrium regimes of the B-C network and their mechanisms in relation to Shields stress θ_0 (or channel aspect ratio β_0), as well as the comparison with a single bifurcation. The widths of the blue lines are scaled with the discharges and the orange arrows indicate the flow directions in each channel. The B-C network refers to the channel network of the "bifurcation-connecting channel".

partitioning at the upstream bifurcation, which is consistent with Figure 5, i.e., the slope advantage tends to more significantly affect the equilibrium configuration of the upstream bifurcation with relatively low Shields stress θ_0 (or channel aspect ratio β_0).

The equilibrium regimes of the B-C network and their mechanisms are briefly summarized in Figure 10. When θ_0 (or β_0) is relatively low (Regime I), the slope advantage is dominant and leads to a higher discharge asymmetry at the upstream bifurcation in the B-C network than a single bifurcation (Figure 5). When θ_0 (or β_0) is relatively high (Regime III), the bifurcation instability is dominant yet the slope advantage mitigates the discharge asymmetry at the upstream bifurcation in the B-C network (Figure 5). For Regime II with moderate θ_0 (or β_0), the dynamic interactions between bifurcation instability and slope advantage lead to the periodic solution (Figure 6).

3.3. Comparison With Previous Studies and Field Observations

Previous studies have shown that the shifting of the dominant branch and hence periodic water partitioning can result from the progradation or aggradation-induced changes in the slope advantage of the two downstream branches (Salter et al., 2018) or migrating bars in the river channels (Bertoldi et al., 2009; Le et al., 2018). In this study, we further showed that the internal dynamics in a channel network can also lead to an oscillatory water partitioning even under constant upstream water and sediment supply as well as fixed downstream relative water level of the receiving basin (Figure 2). These results are robust, as the periodic solution of the B-C network also exists for scenarios adopting the other commonly used nodal-point relation of Wang et al. (1995) as well as longer channels (see the in Supporting Information S1). Furthermore, periodic solution with constant external conditions can also be found in the other dynamical systems such as the generalized Lorenz systems and predator-prey systems (Lipowski, 1999; Shen, 2019).

The historical water partitioning during ebb flows at the upstream bifurcation of the North and South Channels in the Yangtze River Estuary shows an oscillatory pattern that fluctuates around a symmetric configuration and the alternative shifting of the dominant channel from 1958 to 2007 (Gu et al., 2012) (see Figure 11). Our results provide a plausible explanation that the connecting channels, that is, the Nanshatou Passage and Hengsha

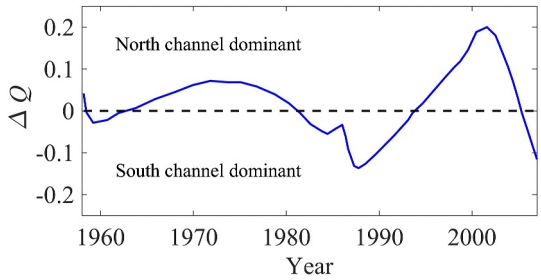

Figure 11. The oscillatory water partitioning at the upstream bifurcation of the north and south channels in the Yangtze River Delta (see Figure 1b). The north channel is dominant when $\Delta Q > 0$, and the south channel is dominant when $\Delta Q < 0$. The original data is from Gu et al. (2012).

Passage, linking the North and South Channels (Figure 1b) play an important role in the development of the oscillatory water partitioning, in addition to those caused by alternating bar formation and in-channel dredging activities (Bertoldi et al., 2009; Le et al., 2018; Wang et al., 2015). The critical role of the connecting channels in preventing a highly asymmetric bifurcation in the Yangtze River Estuary is also suggested by previous studies (Gu et al., 2011, 2012; Wang et al., 2015).

3.4. Implications for the Evolution and Restoration of Deltaic Channel Networks

In this study, we focus on sand-bed channel networks with relatively short branches, in which the wave of bed elevation change migrates relatively fast in the channel (Schielen & Blom, 2018). Therefore, the normal flow and branch-averaged assumptions for the zero-dimensional simulations adopted in this study are valid. Admittedly, the relaxation of the above assumptions in one-dimensional simulations can lead to different oscillatory ranges and periods of the periodic solution as shown in the Supporting Information (Figures S3–S8 in Supporting Information S1). Nonetheless, the mechanisms leading to the different equilibrium regimes in this study are the dynamic interactions between the bifurcation instability and slope advantage modulated by the reversible discharges through the connecting channel (Figure 6); similar interactions are likely to exist in channel networks with longer branches (Figures S5 and S6 in Supporting Information S1), affecting the equilibrium configurations of the channel networks in such cases. Our results, though from a reduced complexity model, open up possibilities for new research into channel networks in rivers, estuaries and deltas with more complex channel structures and processes, such as meandering and bifurcation angle (Kleinhans et al., 2008; Szewczyk et al., 2020) as well as tides (Buschman et al., 2010) through more sophisticated models.

Our results also provide important implications for the planning and restoration of deltaic channel networks. The channel network with a periodic solution can more uniformly nourish deltaic and coastal habitats as it prevents the upstream river discharge and sediment from concentrating into one dominant channel (Edmonds et al., 2011). In particular, the period and amplitude of the periodic solution can help inform the frequency in the shifting of dominant branch and the deviation of water partitioning from a symmetric configuration. While the connecting channels may play an important role in maintaining the dynamics of deltaic channel networks, they can be relatively small and therefore vulnerable to human interventions. Moreover, the periodic and steady-state solutions can coexist for moderate Shields stress (and channel aspect ratio) as shown in Figures 3a and 3b. In such cases, the transition from periodic solution to steady-state solution can occur due to dredging activities (Figure 8). Therefore, a systematic view on the equilibrium configurations of channel networks is also of critical importance for the planning and restoration of the channel networks under pressing environmental changes, as also suggested in Gao et al. (2024).

4. Conclusions

In this study, we studied the equilibrium configurations of a simple yet representative channel network of the "bifurcation-connecting channel" unit through numerical simulations. Our results show that the dynamic interactions between bifurcation instability and water surface slope advantage can lead to the emergence of a periodic solution under moderate Shields stress and channel aspect ratio, in addition to previously identified steady-state solutions. The periodic solution in this study implies a dynamic water partitioning that oscillates around a symmetric partitioning in the channel network under constant boundary conditions, which could provide an additional explanation for the existing field observations. Furthermore, the periodic solution can coexist with the steady-state solution, implying potential shifts between oscillatory and stationary water partitioning patterns under human interventions such as dredging. Our results provide additional insights into the morphological equilibria of complex channel networks in rivers, deltas and estuaries that can help improve their planning and restoration under increasing human interventions.

Data Availability Statement

The code and data are available at a repository on a Zenodo database (Gao, 2023).

Acknowledgments
This work was supported by the National Natural Science Foundation of China (Grants 52388101 and 52239005) and the Program for Guangdong Introducing Innovative and Entrepreneurial Teams (Grant 2019ZT08L213). W. Gao acknowledged the support from the National Natural Science Foundation of China (Grant 52101297).

References

Bertoldi, W., Zanoni, L., Miori, S., Repetto, R., & Tubino, M. (2009). Interaction between migrating bars and bifurcations in gravel bed rivers. *Water Resources Research*, *45*(6), W06418. https://doi.org/10.1029/2008WR007086

Bolla Pittaluga, M., Coco, G., & Kleinhans, M. G. (2015). A unified framework for stability of channel bifurcations in gravel and sand fluvial systems. *Geophysical Research Letters*, *42*(18), 7521–7536. https://doi.org/10.1002/2015GL065175

Bolla Pittaluga, M., Repetto, R., & Tubino, M. (2003). Channel bifurcation in braided rivers: Equilibrium configurations and stability. *Water Resources Research*, *39*(3), 1046. https://doi.org/10.1029/2001WR001112

Buschman, F. A., Hoitink, A. J. F., van der Vegt, M., & Hoekstra, P. (2010). Subtidal flow division at a shallow tidal junction. *Water Resources Research*, *46*(12), W12515. https://doi.org/10.1029/2010WR009266

Dong, T. Y., Nittrouer, J. A., McElroy, B., Il'icheva, E., Pavlov, M., Ma, H. B., et al. (2020). Predicting water and sediment partitioning in a delta Channel Network under varying discharge conditions. *Water Resources Research*, *56*(11), e2020WR027199. https://doi.org/10.1029/2020WR027199

Edmonds, D. A., Chadwick, A. J., Lamb, M. P., Lorenzo-Trueba, J., Murray, A. B., Nardin, W., et al. (2021). Morphodynamic modeling of river-dominated deltas: A review and future perspectives. *Reference module in earth systems and environmental sciences*. Elsevier.

Edmonds, D. A., Paola, C., Hoyal, D. C. J. D., & Sheets, B. A. (2011). Quantitative metrics that describe river deltas and their channel networks. *Journal of Geophysical Research*, *116*(F4), F04022. https://doi.org/10.1029/2010JF001955

Edmonds, D. A., & Slingerland, R. L. (2007). Mechanics of river mouth bar formation: Implications for the morphodynamics of delta distributary networks. *Journal of Geophysical Research*, *112*(F2), F02034. https://doi.org/10.1029/2006JF000574

Engelund, F., & Hansen, E. (1967). *A monograph on sediment transport in alluvial streams*. Teknisk Forlag.

Federici, B., & Paola, C. (2003). Dynamics of channel bifurcations in noncohesive sediments. *Water Resources Research*, *39*(6), 1162. https://doi.org/10.1029/2002WR001434

Gao, W. (2023). Bifurcation interactions lead to periodic water partitioning in A simple deltaic channel network [Dataset]. *Zenodo*. https://doi.org/10.5281/zenodo.10373978

Gao, W., Shao, D., Wang, Z. B., Nardin, W., Yang, W., Sun, T., & Cui, B. (2018). Combined effects of unsteady river discharges and wave conditions on river mouth bar morphodynamics. *Geophysical Research Letters*, *45*(23), 12903–12911. https://doi.org/10.1029/2018GL080447

Gao, W., Shao, D., Wang, Z. B., Zhu, Z., & Yang, Z. (2024). System-wide effects of local bed disturbance on the morphological evolution of a bifurcating channel network. *Journal of Geophysical Research: Earth Surface*, *129*(3), e2023JF007514. https://doi.org/10.1029/2023JF007514

Gao, W., Wang, Z. B., Kleinhans, M. G., Miao, C., Cui, B., & Shao, D. (2023). Floodplain connecting channels as critical paths for hydrological connectivity of deltaic river networks. *Water Resources Research*, *59*(4), e2022WR033714. https://doi.org/10.1029/2022WR033714

Gu, J., Chen, W., Kuang, C. P., Qin, X., & Ma, D. Q. (2011). Influence of Hengsha passage on sediment deposition in the upper reach of the deepwater navigation channel in the Changjiang River Estuary. *Advanced Materials Research*, *255-260*, 3524–3529. https://doi.org/10.4028/www.scientific.net/AMR.255-260.3524

Gu, J., Chen, W., Qin, X., Ma, D. Q., Wang, X. L., & Yang, J. Z. (2012). Analysis on influences of Nanshatou Passage on the deepwater navigation channel of the Changjiang Estuary. *Applied Mechanics and Materials*, *212-213*, 221–224. https://doi.org/10.4028/www.scientific.net/AMM.212-213.221

Hiatt, M., Castaneda-Moya, E., Twilley, R., Hodges, B. R., & Passalacqua, P. (2018). Channel-island Connectivity affects water Exposure time distributions in a coastal River Delta. *Water Resources Research*, *54*(3), 2212–2232. https://doi.org/10.1002/2017WR021289

Hoitink, A. J. F., Nittrouer, J. A., Passalacqua, P., Shaw, J. B., Langendoen, E. J., Huismans, Y., & van Maren, D. S. (2020). Resilience of river deltas in the Anthropocene. *Journal of Geophysical Research: Earth Surface*, *125*(3), e2019JF005201. https://doi.org/10.1029/2019jf005201

Ikeda, S., Parker, G., & Sawai, K. (1981). Bend theory of river meanders 1. Linear development. *Journal of Fluid Mechanics*, *112*(Nov), 363–377. https://doi.org/10.1017/S0022112081000451

Jerolmack, D. J., & Swenson, J. B. (2007). Scaling relationships and evolution of distributary networks on wave-influenced deltas. *Geophysical Research Letters*, *34*(23), L23402. https://doi.org/10.1029/2007gl031823

Jeuken, M. C. J. L., & Wang, Z. B. (2010). Impact of dredging and dumping on the stability of ebb-flood channel systems. *Coastal Engineering*, *57*(6), 553–566. https://doi.org/10.1016/j.coastaleng.2009.12.004

Ke, W. T., Shaw, J. B., Mahon, R. C., & Cathcart, C. A. (2019). Distributary channel networks as moving boundaries: Causes and morphodynamic effects. *Journal of Geophysical Research: Earth Surface*, *124*(7), 1878–1898. https://doi.org/10.1029/2019JF005084

Kleinhans, M. G., de Haas, T., Lavooi, E., & Makaske, B. (2012). Evaluating competing hypotheses for the origin and dynamics of river anastomosis. *Earth Surface Processes and Landforms*, *37*(12), 1337–1351. https://doi.org/10.1002/esp.3282

Kleinhans, M. G., Ferguson, R. I., Lane, S. N., & Hardy, R. J. (2013). Splitting rivers at their seams: Bifurcations and avulsion. *Earth Surface Processes and Landforms*, *38*(1), 47–61. https://doi.org/10.1002/esp.3268

Kleinhans, M. G., Jagers, H. R. A., Mosselman, E., & Sloff, C. J. (2008). Bifurcation dynamics and avulsion duration in meandering rivers by one-dimensional and three-dimensional models. *Water Resources Research*, *44*(8), W08454. https://doi.org/10.1029/2007WR005912

Kleinhans, M. G., & van den Berg, J. H. (2011). River channel and bar patterns explained and predicted by an empirical and a physics-based method. *Earth Surface Processes and Landforms*, *36*(6), 721–738. https://doi.org/10.1002/esp.2090

Konkol, A., Schwenk, J., Katifori, E., & Shaw, J. B. (2022). Interplay of river and tidal forcings promotes loops in coastal channel networks. *Geophysical Research Letters*, *49*(10), e2022GL098284. https://doi.org/10.1029/2022GL098284

Le, T. B., Crosato, A., Mosselman, E., & Uijttewaal, W. S. J. (2018). On the stability of river bifurcations created by longitudinal training walls. Numerical investigation. *Advances in Water Resources*, *113*, 112–125. https://doi.org/10.1016/j.advwatres.2018.01.012

Lipowski, A. (1999). Oscillatory behavior in a lattice prey-predator system. *Physical Review E*, *60*(5), 5179–5184. https://doi.org/10.1103/PhysRevE.60.5179

Moodie, A. J., & Passalacqua, P. (2021). When does faulting-induced subsidence drive distributary network reorganization? *Geophysical Research Letters*, *48*(22), e2021GL095053. https://doi.org/10.1029/2021GL095053

Nanson, G. C., & Knighton, A. D. (1996). Anabranching rivers: Their cause, character and classification. *Earth Surface Processes and Landforms*, *21*(3), 217–239. https://doi.org/10.1002/(SICI)1096-9837(199603)21:3<217::AID-ESP611>3.0.CO;2-U

Ragno, N., Redolfi, M., & Tubino, M. (2021). Coupled morphodynamics of river bifurcations and confluences. *Water Resources Research*, *57*(1), e2020WR028515. https://doi.org/10.1029/2020WR028515

Ragno, N., Redolfi, M., & Tubino, M. (2022a). Quasi-universal length scale of river Anabranches. *Geophysical Research Letters*, *49*(16), e2022GL099928. https://doi.org/10.1029/2022GL099928

Ragno, N., Tambroni, N., & Bolla Pittaluga, M. (2020). Effect of small tidal Fluctuations on the stability and equilibrium configurations of bifurcations. *Journal of Geophysical Research-Earth Surface*, *125*(8), e2020JF005584. https://doi.org/10.1029/2020JF005584

Ragno, N., Tambroni, N., & Pittaluga, M. B. (2022b). Competing feedback in an idealized tide-influenced delta network. *Environmental Fluid Mechanics*, *22*(2–3), 535–557. https://doi.org/10.1007/s10652-022-09857-2

Redolfi, M., Zolezzi, G., & Tubino, M. (2019). Free and forced morphodynamics of river bifurcations. *Earth Surface Processes and Landforms*, *44*(4), 973–987. https://doi.org/10.1002/esp.4561

Riquier, J., Piégay, H., Lamouroux, N., & Vaudor, L. (2017). Are restored side channels sustainable aquatic habitat features? Predicting the potential persistence of side channels as aquatic habitats based on their fine sedimentation dynamics. *Geomorphology*, *295*, 507–528. https://doi.org/10.1016/j.geomorph.2017.08.001

Salter, G., & Lamb, M. P. (2022). Autocyclic Secondary channels stabilize deltaic islands undergoing relative sea level rise. *Geophysical Research Letters*, *49*(15), e2022GL098885. https://doi.org/10.1029/2022GL098885

Salter, G., Paola, C., & Voller, V. R. (2018). Control of delta avulsion by downstream sediment Sinks. *Journal of Geophysical Research-Earth Surface*, *123*(1), 142–166. https://doi.org/10.1002/2017JF004350

Salter, G., Voller, V. R., & Paola, C. (2020). Chaos in a simple model of a delta network. *Proceedings of the National Academy of Sciences of the United States of America*, *117*(44), 27179–27187. https://doi.org/10.1073/pnas.2010416117

Schielen, R. M. J., & Blom, A. (2018). A reduced complexity model of a gravel-sand river bifurcation: Equilibrium states and their stability. *Advances in Water Resources*, *121*, 9–21. https://doi.org/10.1016/j.advwatres.2018.07.010

Shaw, J. B., Mason, K. G., Ma, H., & McCain, G. W. III. (2021). Influences on discharge partitioning on a large river delta: Case study of the Mississippi-Atchafalaya diversion, 1926–1950. *Water Resources Research*, *57*(5), e2020WR028090. https://doi.org/10.1029/2020WR028090

Shen, B. W. (2019). Aggregated Negative feedback in a generalized Lorenz model. *International Journal of Bifurcation and Chaos*, *29*(3), 1950037. https://doi.org/10.1142/S0218127419500378

Sinha, S. K., & Parker, G. (1996). Causes of concavity in longitudinal profiles of rivers. *Water Resources Research*, *32*(5), 1417–1428. https://doi.org/10.1029/95wr03819

Swinkels, C. M., Jeuken, C. M. C. J. L., Wang, Z. B., & Nicholls, R. J. (2009). Presence of connecting channels in the western scheldt estuary. *Journal of Coastal Research*, *25*(3), 627–640. https://doi.org/10.2112/06-0719.1

Szewczyk, L., Grimaud, J. L., & Cojan, I. (2020). Experimental evidence for bifurcation angles control on abandoned channel fill geometry. *Earth Surface Dynamics*, *8*(2), 275–288. https://doi.org/10.5194/esurf-8-275-2020

Talmon, A. M., Struiksma, N., & Van Mierlo, M. C. L. M. (1995). Laboratory measurements of the direction of sediment transport on transverse alluvial-bed slopes. *Journal of Hydraulic Research*, *33*(4), 495–517. https://doi.org/10.1080/00221689509498657

Tejedor, A., Longjas, A., Edmonds, D. A., Zaliapin, I., Georgiou, T. T., Rinaldo, A., & Foufoula-Georgiou, E. (2017). Entropy and optimality in river deltas. *Proceedings of the National Academy of Sciences of the United States of America*, *114*(44), 11651–11656. https://doi.org/10.1073/pnas.1708404114

van Denderen, R. P., Schielen, R. M. J., Blom, A., Hulscher, S. J. M. H., & Kleinhans, M. G. (2018). Morphodynamic assessment of side channel systems using a simple one-dimensional bifurcation model and a comparison with aerial images. *Earth Surface Processes and Landforms*, *43*(6), 1169–1182. https://doi.org/10.1002/esp.4267

Wang, Z. B., De Vries, M., Fokkink, R. J., & Langerak, A. (1995). Stability of river bifurcations in 1D morphodynamic models. *Journal of Hydraulic Research*, *33*(6), 739–750. https://doi.org/10.1080/00221689509498549

Wang, Z. B., Van Maren, D. S., Ding, P. X., Yang, S. L., Van Prooijen, B. C., De Vet, P. L. M., et al. (2015). Human impacts on morphodynamic thresholds in estuarine systems. *Continental Shelf Research*, *111*, 174–183. https://doi.org/10.1016/j.csr.2015.08.009

Wang, Z. B., Wang, Z. Y., & de Vriend, H. J. (2008). Impact of water diversion on the morphological development of the Lower Yellow River. *International Journal of Sediment Research*, *23*(1), 13–27. https://doi.org/10.1016/S1001-6279(08)60002-5